J. Fluid Mech. (1978), *vol.* 87, *part* 3, *pp.* 475–496
Printed in Great Britain

Experimental investigation of the supersonic flow past a slender cone at high incidence

By C. NEBBELING AND W. J. BANNINK

Department of Aerospace Engineering, University of Technology, Delft, The Netherlands

(Received 7 December 1977)

The supersonic flow field past a circular cone of semi-apex angle 7·5° at incidences up to 26° has been investigated experimentally at a free-stream Mach number of 2·94. The experiments were made using a five-hole conical-head directional probe. Since the flow past the cone was found to be conical, the flow phenomena may be described in a plane perpendicular to the cone axis. This paper gives the direction of the conical streamlines, the conical sonic line and the conical Mach number in such a plane, all of which may be deduced from the measurements. At incidences exceeding twice the cone semi-apex angle a separated flow regime was observed which consisted of two main vortices on either side of the leeward plane of symmetry, and probably also two secondary vortices close to the cone surface. From incidences of 17° onwards, an embedded region of conical supersonic flow terminated by a shock wave was revealed. At 22°, approximately, a second embedded shock wave was measured close to the cone surface and extended slightly across the leeward plane of symmetry. This shock wave may have been generated by the vortex system, which induced supersonic cross-flow components towards the cone.

1. Introduction

The investigation of the flow field past cones at high angles of incidence is of considerable theoretical as well as experimental interest. Numerical solutions have yielded good results for rather small angles of incidence, where no flow separation occurs and where one may consider the flow to be inviscid. In the present investigation we are concerned with the flow field past cones at high angles of incidence; for the inviscid case, numerical results have been presented by Holt & Ndefo (1970), Kutler & Lomax (1971) and Fletcher (1975). At these high incidences, however, viscous effects play a dominant role, especially on the leeward side of the cone. The flow field is more complicated and numerical calculations of the inviscid flow field are only partially in agreement with experiments. Tracy (1963) showed for the first time the complexity of the flow field at high angles of incidence and after him several others (Guffroy *et al.* 1968; Rainbird 1968; Feldhuhn & Winkelmann 1969; Feldhuhn, Winkelmann & Pasiuk 1970; Yahalom 1971; Stetson 1972; Houwink 1974; Zakkay & Alzner 1974) confirmed the strong viscous–inviscid interaction on the leeward side of the cone. Even at angles of incidence below the cone half-angle, cross-flow separation was observed. At higher incidences a system of counterrotating vortices developed in the separated region. Over a wide range of Mach numbers, from low supersonic to

hypersonic, and for cone half-angles ranging from about 5° to 20°, these effects are quite similar.

Calculations by Lubard & Helliwell (1973) and Massot (1976), in which an approximation of the steady-state Navier–Stokes equations was used, show the formation of vortices in the separated zone. Reasonable agreement was found with Tracy's experiments. Since it may be expected that in the near future the interaction of viscous and inviscid flow will be calculated more accurately, further experimental data will be needed to check theoretical results and to obtain a better understanding of these flow phenomena.

In the present paper measurements of the flow field about a cone at several angles of incidence are presented. One of the most important aims was to achieve a detailed impression of the velocity distribution in the flow field, so that regions with flow separation and vortices could be clearly indicated, as well as the regions of conical subsonic and supersonic flow. The experiments were performed using a five-hole conical-head probe which measures the Pitot pressure as well as the flow angle. In addition to the flow-field measurements, surface flow pictures were also made.

2. Experimental apparatus

2.1. *Test facilities and models*

The experiments were made in two supersonic blow-down wind tunnels in the Department of Aerospace Engineering, University of Technology, Delft: the TST 27 and the ST 15, which have test sections of cross-section $0{\cdot}27 \times 0{\cdot}27$ m and $0{\cdot}15 \times 0{\cdot}15$ m, respectively. The TST 27 wind tunnel is equipped with a variable nozzle and operates in the Mach number range 0·5–5·5, approximately. The maximum value of the settling chamber pressure is 40 bars. The TST 27 was used to provide surface flow visualization at different angles of incidence of the cone model and at different Mach numbers. Also, some of the schlieren pictures were made in this wind tunnel.

The flow-field measurements have been made in the ST 15 wind tunnel, which has fixed nozzle blocks. The free-stream Mach number, determined from Pitot-pressure measurements, had a mean value of 2·94 with local variations in the test section of less than 0·3 %. During the measurements the settling-chamber pressure was kept constant at a value of $5{\cdot}35 \pm 0{\cdot}03$ bars. The specific humidity in the storage vessel for both wind tunnels was measured to be $0{\cdot}86 \times 10^{-4}$ kg/kg.

For flow-visualization tests, in the TST 27 wind tunnel, a cone of semi-apex angle 7·5° and length 25 cm was used. The technique for obtaining two-dimensional pictures of the flow pattern on the conical surface is described in § 2.3.

The cone model used in the flow-field measurements again had a semi-apex angle of 7·5° but was of length 15 cm. The cone apex of this model was very slightly blunted. The reason for this is that a perfectly conical apex is very vulnerable and that previous measurements had shown that the flow symmetry is markedly affected by a very small deformation of the nose point, almost invisible to the naked eye. Comparative tests confirmed that the slight rounding of the nose point did not noticeably affect the conical behaviour of the flow.

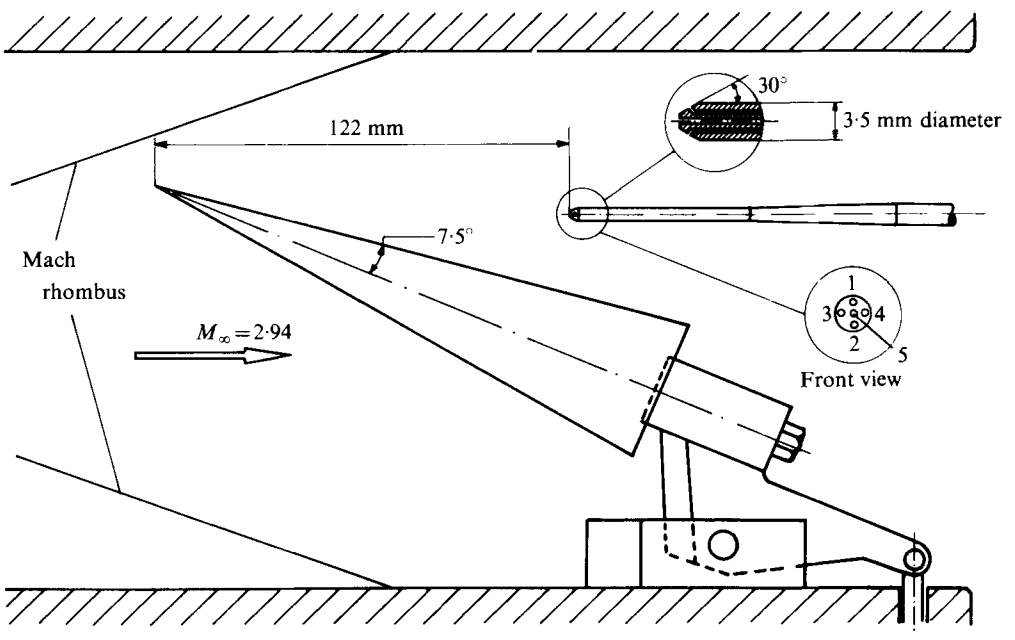

FIGURE 1. Test arrangement.

2.2. *Conical-head probe*

The flow-field measurements in the ST 15 wind tunnel were made with a conical-head probe (figure 1) with a diameter of 3·5 mm and a semi-apex angle of 30°. The conical part of the probe was provided with four static-pressure orifices at an angular displacement of 90°; also, a central orifice was fitted, serving as a Pitot-pressure tap. The pressure orifices had a diameter of 0·3 mm and the distance between two opposite holes was 1·54 mm. The calibration of the probe is described in the appendix.

2.3. *Surface flow visualization*

To produce the surface flow patterns, a mixture consisting of 30 g of Shell Tellus 29 (oil), 19 g of titanium dioxide and 4 drops of Shell T40 (detergent) was used. Shell T40 was chosen as the detergent instead of the commonly used oil-acid because of its durability. The oil mixture was thinly and evenly spread on the cone model. With the exception of the nose point, the conical surface of the model was covered with a thin layer of adhesive plastic foil. A small backward-facing step, corresponding to the thickness of the foil, had been machined in the surface of the cone at the nose, so that after application of the foil the entire surface was smooth and free from steps.

A satisfactory oil flow pattern formed after a running time of about 20 s, depending on the Mach number of the flow. After the run, and after some time had been allowed for the model to regain room temperature (the plastic foil being rather brittle at the low temperature of the model at the end of the run), the plastic foil was carefully unwrapped from the surface and spread out flat for photography of the pattern.

3. Description of the tests

3.1. *Data acquisition*

All pressures were measured with Statham pressure transducers with appropriate ranges. A thermocouple was used to determine the stagnation temperature in the settling chamber relative to the temperature of melting ice.

The five-hole probe was mounted on a traversing mechanism which was driven by three stepping motors and allowed traverses in small increments in three directions. The displacement in the lateral direction (normal to the vertical plane of symmetry) was obtained by counting the number of steps (0·015 mm per step) from a well-defined reference position inside the test section. As the position of the probe in the vertical plane was influenced by deflexion of the probe and support under load, the actual position of the probe was determined optically during the run, using a vertical and horizontal cathetometer.

All data were automatically recorded on punched tape by a digital recording system, with the exception of the cathetometer readings, which were entered by hand. The recorded data were processed off-line by the University IBM 370/158 computer.

3.2. *Measurements*

Before the field measurements were started, a survey of the flow in the empty test section was made with the five-hole probe. It was ascertained that, at the chosen position of the model, no discrete disturbances were present in the planes in which the actual field measurements were to be carried out. Equally important was the determination of the flow direction in the empty test section: a downwash of 0·2° was measured. The actual field measurements were made at $M = 2{\cdot}94$ in the flow field of a cone of semi-apex angle 7·5° at incidences of 7·5°, 12·4°, 17·3°, 22·4° and 25·0°. These incidences were measured optically during the runs.

An outline of the test arrangement is given in figure 1. The five-hole probe could not be mounted exactly parallel to the wind-tunnel axis. Measurements indicated an angle of incidence of $-0{\cdot}33°$ and a yaw angle of $-0{\cdot}19°$. Corrections for these deviations have been applied in the data reduction computer program.

Houwink (1974), using exactly the same model arrangement, showed that for angles of incidence below 25° the flow field past the cone was essentially conical. A superficial check in the present case confirmed his results. Schlieren photographs also supported the assumption of conical flow. Therefore measurements were made in only one plane, normal to the wind-tunnel axis and at about 125 mm downstream of the apex of the cone. The probe was traversed normal to the plane of symmetry at intervals of 1·5 mm, this interval corresponding to the lateral distance between the central hole of the probe and a pressure tap on its conical surface. After each step, and after a sufficient time lag for pressure equalization, the five probe pressures were read, together with the settling-chamber pressure, the settling-chamber temperature, a reference Pitot pressure in the undisturbed part of the test section and the lateral position of the probe. These traverses were made at levels with a vertical spacing of about 1·5 mm.

During each run the vertical and streamwise positions of the probe were measured optically with an accuracy of 0·03 mm. To check the symmetry of the flow field above the cone, the traverses started at 15 mm beyond the plane of symmetry and extended to 6 mm across the bow shock wave of the cone.

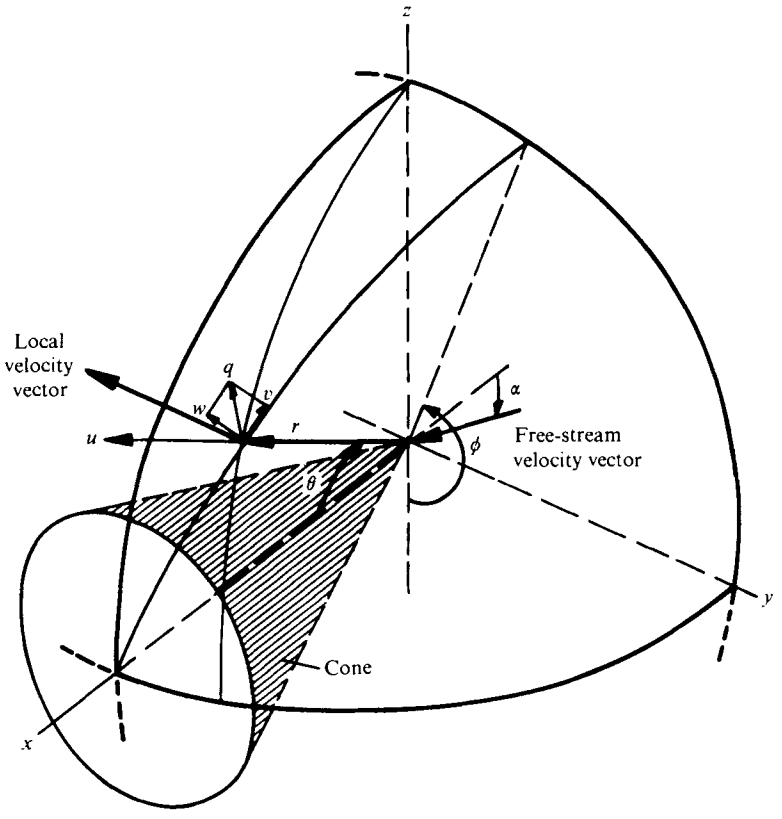

FIGURE 2. Spherical (conical) co-ordinate system and velocity components.

4. Data reduction

The results of the measurements are presented in a spherical co-ordinate system with its origin at the apex of the cone, the reference axis coinciding with the cone axis. The reference plane is the plane of symmetry through the cone axis and the free-stream velocity vector. In this system the three co-ordinates are r, θ and ϕ (figure 2). The components of the local velocity are u, in the radial direction, v, in the meridional plane and normal to the local ray through the cone apex, and w, normal to u and v. The total component normal to a ray is called the conical velocity q. The conical Mach number M_c is defined as the ratio of the conical velocity to the local speed of sound.

In the flow field past the cone the local Mach number and the direction of the flow with respect to the probe axis have been determined from the probe pressures only. The local Mach number results from the calibrated ratio of the Pitot pressure p_p to the average p_s of the four cone surface pressure headings. To use this calibration, the angle θ_p between the local velocity vector and the probe axis must be known. This angle is calculated from the super-ellipse relation given in the appendix by (A 3), which for $\theta = \theta_p$ reads

$$\left[\frac{(p_2-p_1)/p_5-[A_0]_{\phi=0}}{[F_1(\theta_p)-A_0]_{\phi=0}}\right]^{n(\theta_p,M)}+\left[\frac{(p_4-p_3)/p_5-(B_0)_{\phi=90°}}{[F_2(\theta_p)-B_0]_{\phi=90°}}\right]^{n(\theta_p,M)}=1. \qquad (1)$$

It will be observed that the exponent n in this relation depends on the as yet unknown Mach number. The influence of the Mach number is, however, small. As a first approximation, the Mach number is taken as that corresponding at $\theta_p = 0$ to the ratio of the Pitot pressure p_5 to the average of the four circumferential pressures $p_1, \ldots, p_4$. Using this Mach number, θ_p is obtained from (A 7) (see appendix) and this value is used to obtain the corrected Mach number from the calibration. Introducing the corrected Mach number in (A 7) yields a corrected value of θ_p; this value is taken as the final approximation.

The local static pressure in the flow field is determined from the Mach number and the Pitot pressure, which is obtained from p_5 and the pitch angle θ_p (see (A 6) for $\theta = \theta_p$). The local speed of sound is derived from the Mach number and the settling-chamber temperature, assuming constant stagnation enthalpy in the wind-tunnel flow

The meridional angle ϕ_p of the velocity vector is obtained from the relation

$$\phi_p = \tan^{-1}\left[\frac{p_2 - p_1}{p_4 - p_3}\right]. \tag{2}$$

Inaccuracies in the results due to the finite dimensions of the probe are compensated for by using an interpolation scheme such that the four cone static pressures are obtained at the location of the central orifice of the probe. As an additional advantage of the interpolation procedure, the influence of flow divergence on the calibration is also eliminated. In a divergent flow the apparent probe cone angle differs from the actual angle, which results in variation of the probe characteristics; in particular, the local Mach number determined from the measurements is rather sensitive to the apparent probe cone angle.

From the measured flow quantites and from the known position and inclination of the probe with respect to the cone, the components u, v and w in the spherical co-ordinate system may be determined. Because of the conical nature of the flow field, it is convenient to analyse this kind of flow on a unit sphere centred at the origin of the conical field. On the unit sphere a conical streamline may be defined as a line to which the conical velocity component is tangential at every point. The conical Mach number is calculated from the measured Mach number, the position of the probe and the direction of the local velocity vector using the expression

$$M_c = M[\sin^2\theta_f \sin^2(\phi - \phi_f) + \{\sin\theta_f \cos(\phi - \phi_f)\cos\theta - \cos\theta\sin\theta\}^2]^{\frac{1}{2}}, \tag{3}$$

where θ and ϕ are the co-ordinates of a point on the unit sphere and θ_f and ϕ_f indicate the direction of the local velocity vector with respect to the co-ordinate system.

In order to represent the data in a plane normal to the cone axis, the velocity components are projected along rays through the origin by means of central projection. In this plane a horizontal (y) axis and a vertical (z) axis are defined; the Cartesian co-ordinates with respect to these axes are then non-dimensionalized by the local radius R of the cone cross-section. The central projection of the velocity components implies the possibility of tracing the conical streamlines. The slope of the conical streamlines is given by

$$\tan\gamma = \frac{-\sin\theta_f \cos\phi_f - (z/R)\cos\theta_f \tan\theta_c}{\sin\theta_f \sin\phi_f - (y/R)\cos\theta_f \tan\theta_c}, \tag{4}$$

where γ is the angle with the $+y$ axis and θ_c the semi-apex angle of the cone.

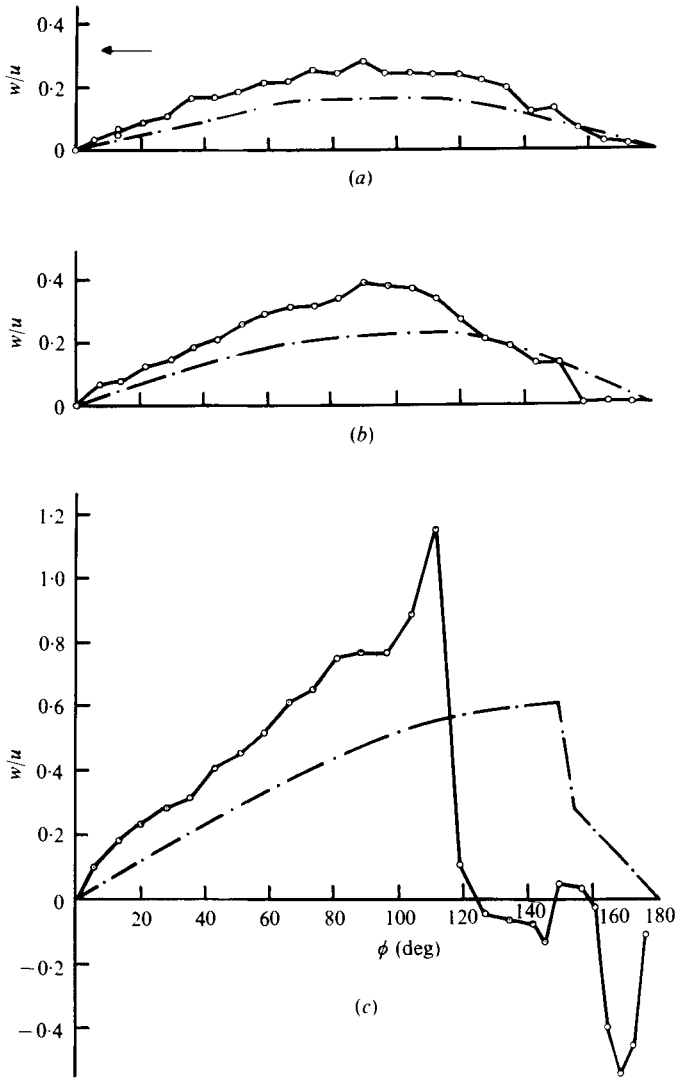

FIGURE 4. Angular direction of surface streamlines compared with inviscid theory. ○, experiment; —·—, inviscid theory; ←, windward side. (*a*) $\alpha = 6°$, (*b*) $\alpha = 8°$, (*c*) $\alpha = 17{\cdot}3°$.

5. Results

5.1. *Surface flow*

Figure 3 (plates 1 and 2) shows photographs of the surface flow patterns. The straight outer edges of the unwrapped patterns represent the windward symmetry plane of the cone while the central part corresponds to the leeward side.

The first evidence of flow separation is observed at an angle of incidence α of about 10° (figure 3*a*), when the oil flows together in a narrow region on either side of the symmetry plane. Also, reattachment of the flow appears on the leeward symmetry plane, suggesting the development of a symmetrical vortex system. At $\alpha = 12°$ (figure 3*b*) four separation lines are visible; the two innermost may indicate a

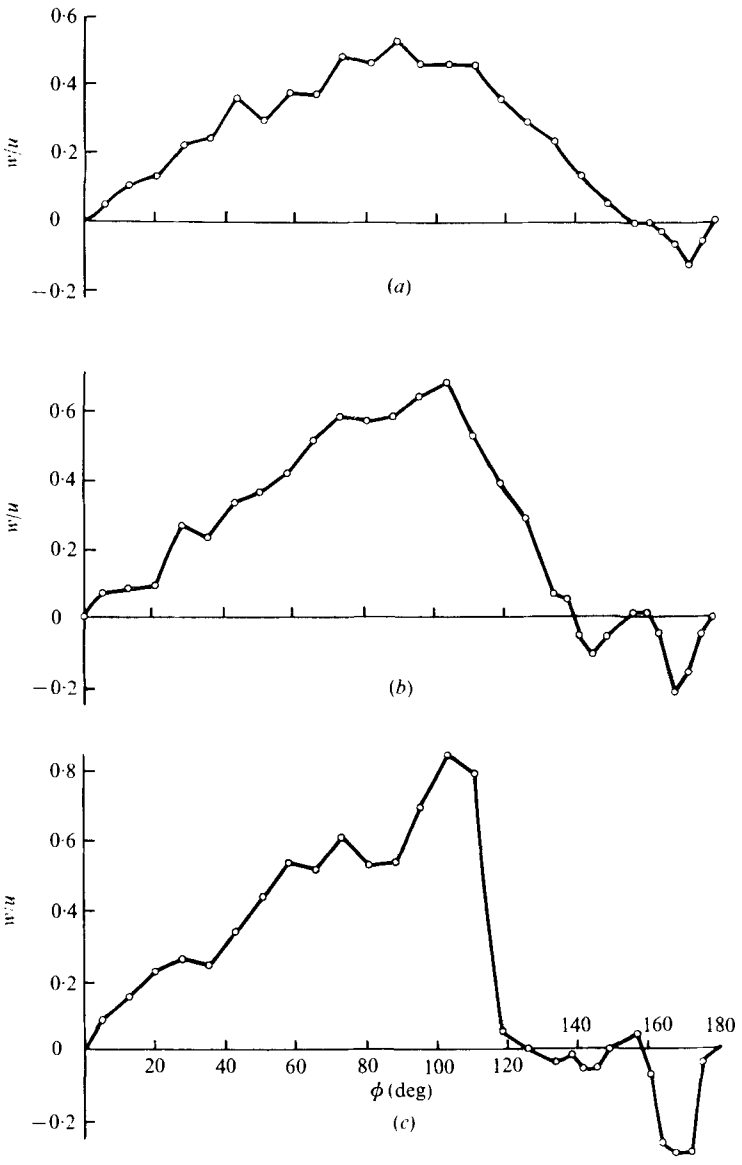

FIGURES 5(a–c). For legend see opposite.

secondary vortex system inside a primary region of separated flow. At $\alpha = 14°$ the separation lines have developed into sharp lines (figure 3*c*), and this flow pattern is maintained up to an incidence of about 26° (figure 3*d*). Houwink (1974) showed the existence of asymmetrical effects at angles of incidence exceeding 28°.

In figures 4 and 5 the direction w/u of the shear stress determined from the oil-flow pictures is given as a function of the circumferential angle, where u is the velocity component along a generator of the cone and w the velocity component in the circumferential direction. Figures 4 (*a*)–(*c*) show the measured shear-stress distribution compared with inviscid theory. The angle of the measured surface streamlines with respect to a generator is larger than in the inviscid case since, owing to the absence of a pressure

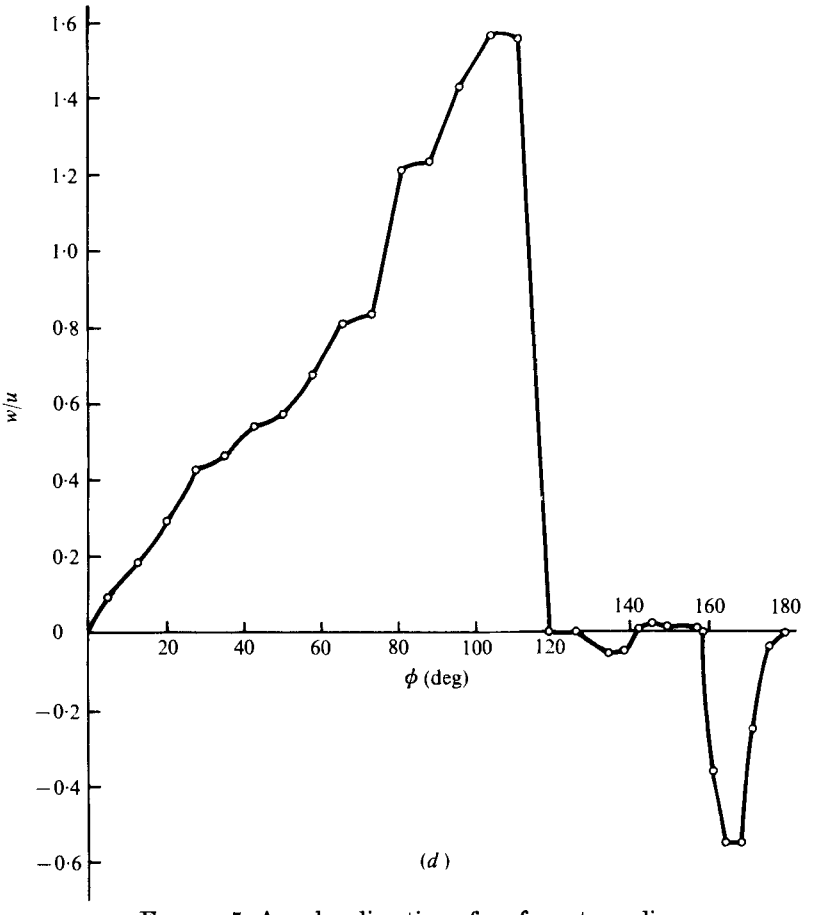

FIGURE 5. Angular direction of surface streamlines.
(*a*) $\alpha = 10°$, (*b*) $\alpha = 12°$, (*c*) $\alpha = 14°$, (*d*) $\alpha = 26°$.

gradient along a generator, the secondary flow in the sublayer of the boundary layer is dominated by the circumferential pressure gradient.

The abrupt changes in the direction of the shear stress at $\alpha = 14°$ (figure 5*c*) may indicate the existence of an embedded shock wave standing on the cone surface at a circumferential angle ϕ of about 120°. From $\alpha = 12°$ to 14° the flow may be considered to be in a state of transition from a structure which depends strongly on the incidence to one which is almost independent of α. For values of α larger than 14° approximately, a flow structure with several pronounced separations and reattachments occurs.

Increasing the angle of incidence still further does not change the surface flow structure significantly until $\alpha = 26°$ (figure 5*d*). It seems that the embedded shock wave stabilizes the flow structure up to that angle of incidence. At $\alpha = 17{\cdot}3°$ (figure 4*c*) the direction of the shear stress calculated for inviscid flow using a shock-capturing technique changes abruptly at $\phi \approx 150°$, which corresponds to the calculated location of the shock wave in this flow field. Although in this respect there seems to be some agreement, the structure of the measured flow field is completely different from that of the calculated field, as may be seen in the following.

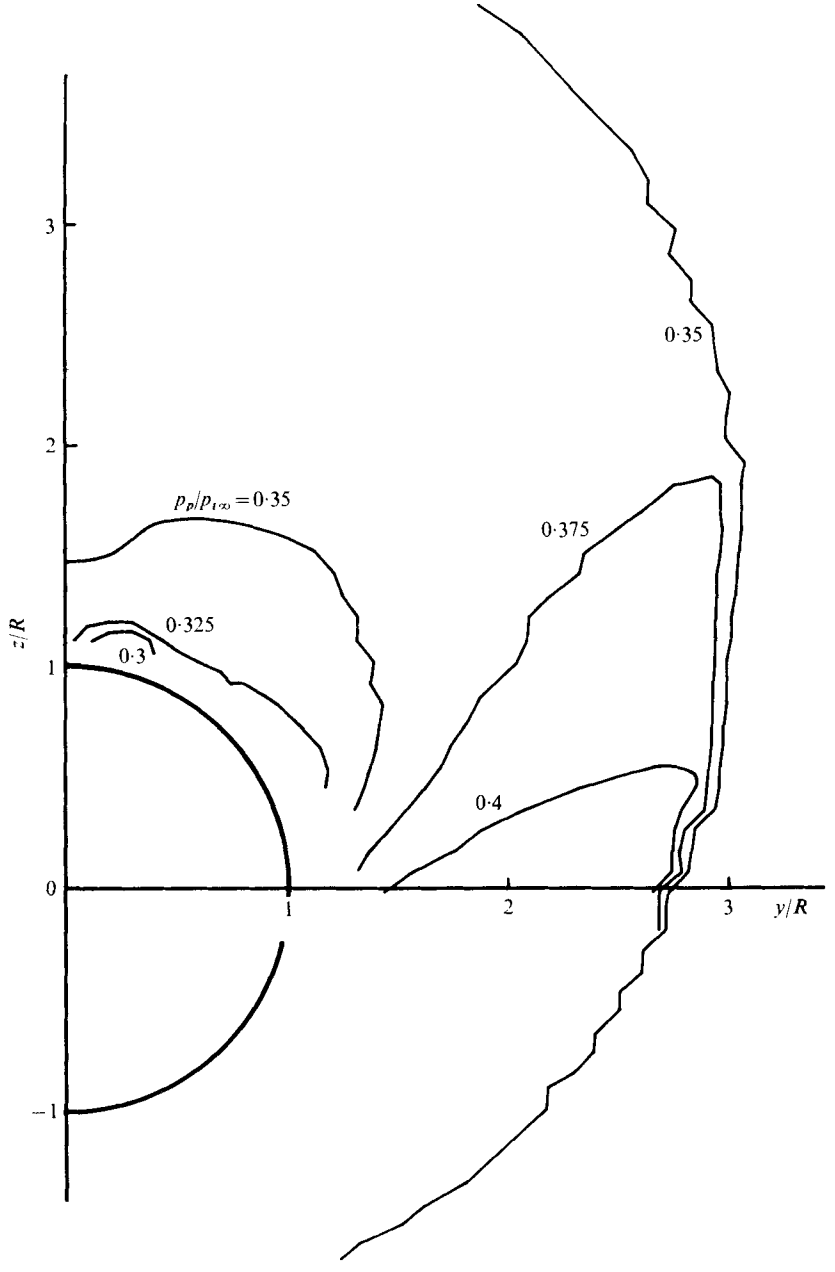

FIGURE 6. Lines of constant Pitot pressure at $\alpha = 12{\cdot}4°$ ($p_{t\infty}$ = free-stream stagnation pressure).

5.2. *Flow field*

Pitot pressure distribution. In figure 6 lines of constant Pitot pressure (non-dimensionalized by the free-stream stagnation pressure) are given for $\alpha = 12{\cdot}4°$; no regions of strong gradients are observed.

At $\alpha = 17{\cdot}3°$ the Pitot pressure distribution in the flow field is of a more pronounced

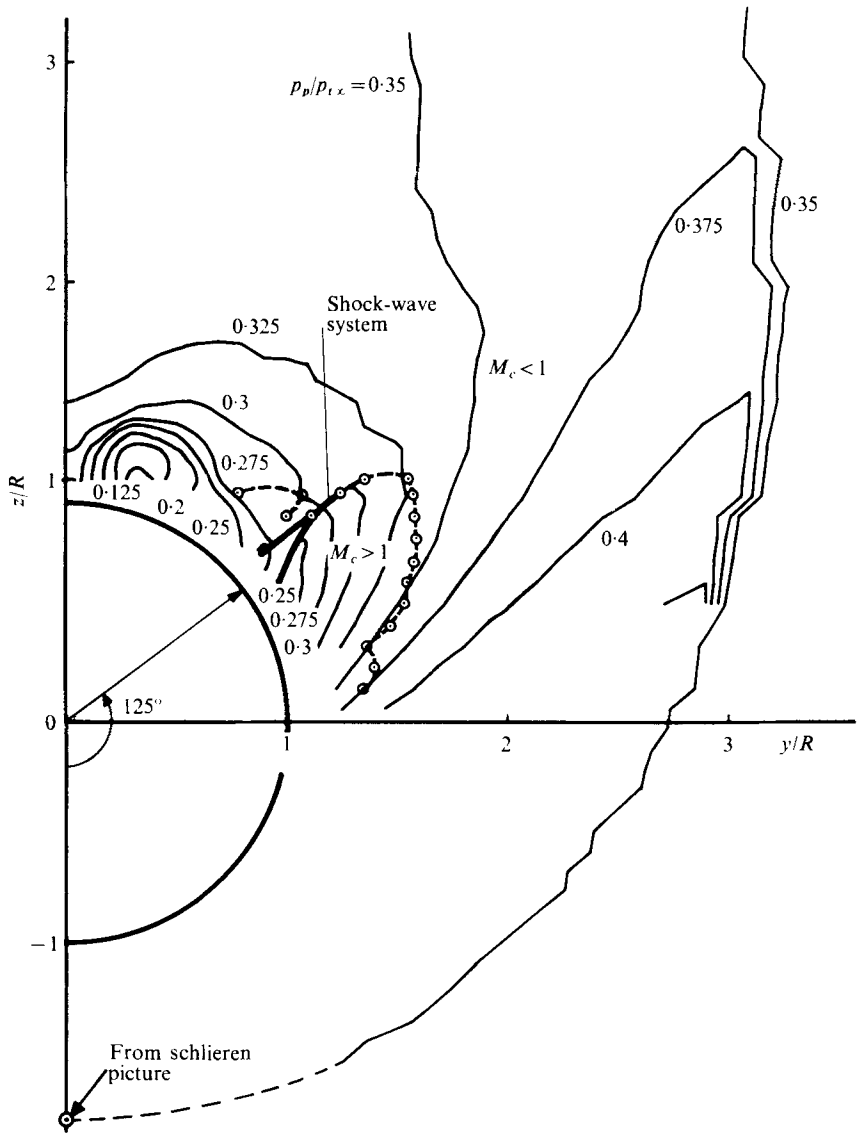

FIGURE 7. Lines of constant Pitot pressure, embedded shock-wave system and conical sonic line at $\alpha = 17{\cdot}3°$. ⊙---⊙, conical sonic line.

nature (figure 7). At the leeward side, the isobars surround a region of very low Pitot pressure. At a circumferential angle of about 125°, meandering of the isobars indicates the existence of two shock waves, which form together a lambda shock wave, a well-known phenomenon in supersonic separated flows.

At an angle of incidence of 22·4° the low Pitot pressure region has developed into a pressure field similar to that of a vortex core; see figure 8. The Pitot pressure in the centre of the region of concentric isobars is very low with a minimum value of $p_p/p_{t\infty}$ of about 0·07, $p_{t\infty}$ being the free-stream stagnation pressure. The question arises whether it is possible to have a conical vortex in the flow field, i.e. a vortex satisfying the conditions for conical flow, which in turn implies that the vortex strength depends

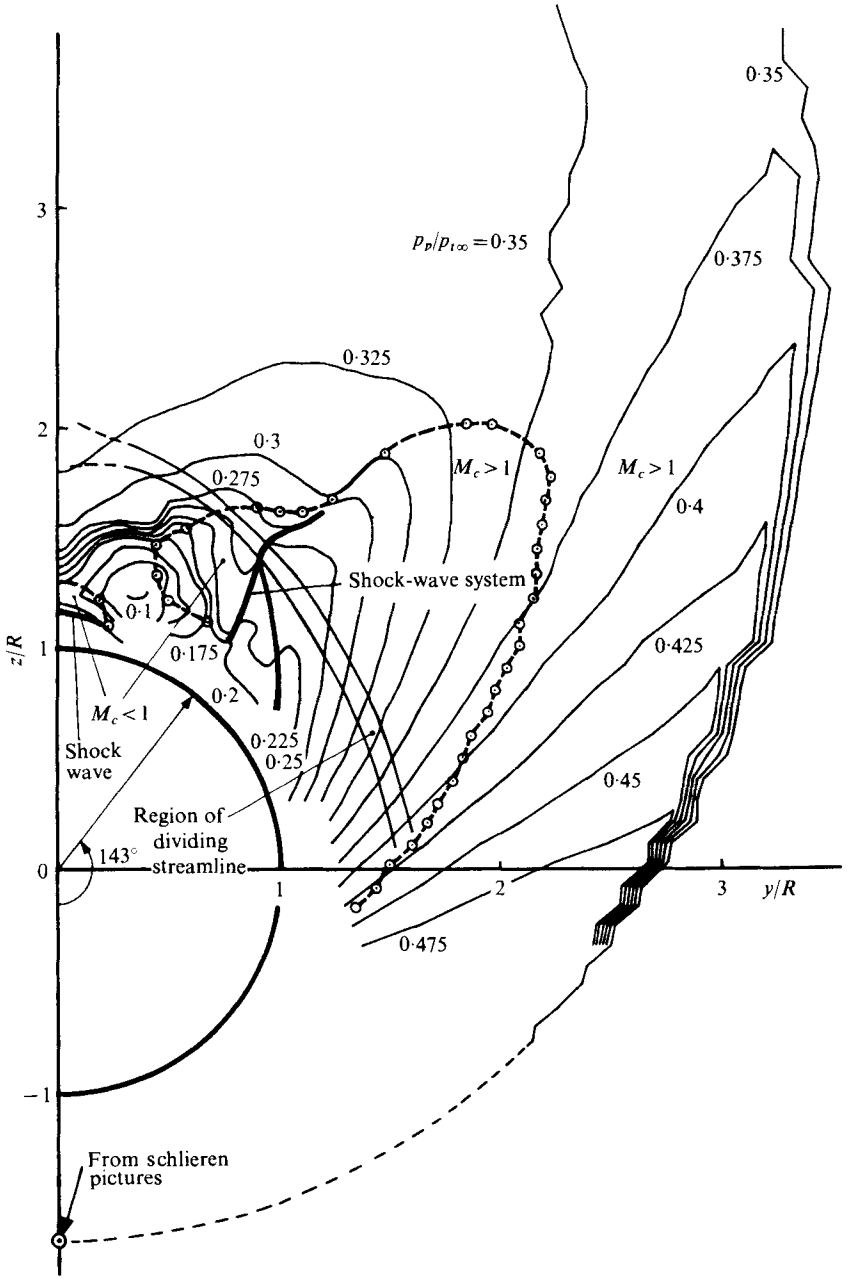

FIGURE 8. Lines of constant Pitot pressure, embedded shock waves, conical sonic line and region of dividing streamline at $\alpha = 22{\cdot}4°$. ⊙···⊙, conical sonic line.

linearly on the distance to the conical centre. The present measurements give evidence to that effect, although more research is required to answer the question completely.

At an angle of incidence of 22·4° the embedded shock waves are located at a circumferential angle of about 143°. The lambda structure still exists, but a new feature appears. Halfway along the shock wave a strong change in curvature may be

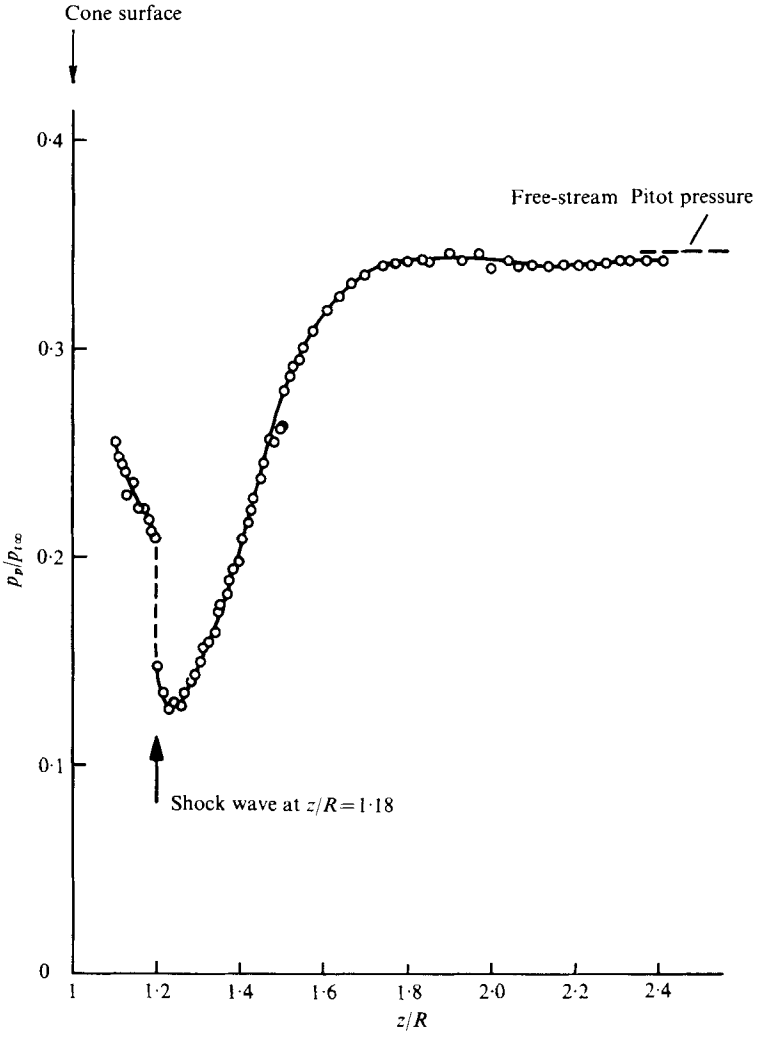

FIGURE 9. Pitot pressure distribution in the leeward plane of symmetry at $\alpha = 22{\cdot}4°$.

seen, whereas no sudden change in the flow direction has been measured. Moreover, figure 8 shows that the strong curvature of the shock wave is located at the intersection with the streamline dividing the flow field into two regions: one that may be considered inviscid and one that is dominated by vortex flow (see also figure 13). This supports the suggestion that the upper and lower parts of the shock wave are generated by different effects. The lower part may be generated by the flow separation from the cone surface, whereas the upper part is necessary to satisfy the boundary conditions in the inviscid flow. The two parts merge smoothly into each other. The upper part of the flow field may be computed by considering the flow about a conical body whose cross-section is bounded by the above-mentioned dividing streamline. This approach was followed, more or less, by Zakkay & Alzner (1974) and Nakao (1975).

A detailed impression of the Pitot-pressure distribution in the leeward plane of

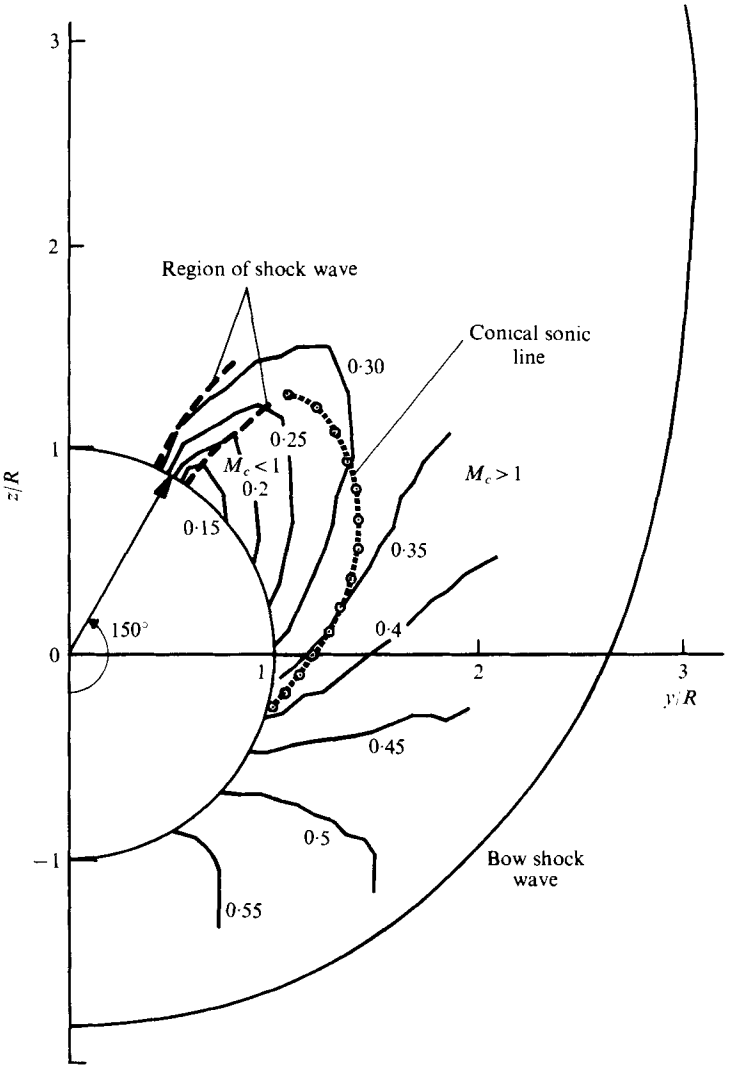

FIGURE 11. Lines of constant Pitot pressure, conical sonic line and region of embedded shock wave computed by a shock-capturing technique. $\alpha = 17{\cdot}3°$.

symmetry is shown in figure 9, along with additional measurements with a small flattened Pitot probe at a slightly smaller angle of incidence. A shock wave has been measured as a jump in the Pitot pressure at a distance above the cone of $z/R = 1{\cdot}2$, a position corresponding to that of the shock wave just above the cone surface observed in the schlieren photograph in figure 10 (plate 3).

Embedded shock waves and the distribution of the conical Mach number. At an angle of incidence $\alpha = 12{\cdot}4°$ the flow field between the bow wave and the cone appears to be conical subsonic and no embedded shock waves are found. At $\alpha = 17{\cdot}3°$ the flow contains a conical supersonic region (figure 7) which is enclosed partly by a conical sonic line and partly by a lambda-type shock wave. Downstream of the shock wave a second conical supersonic region has been measured but is not quite understood. The

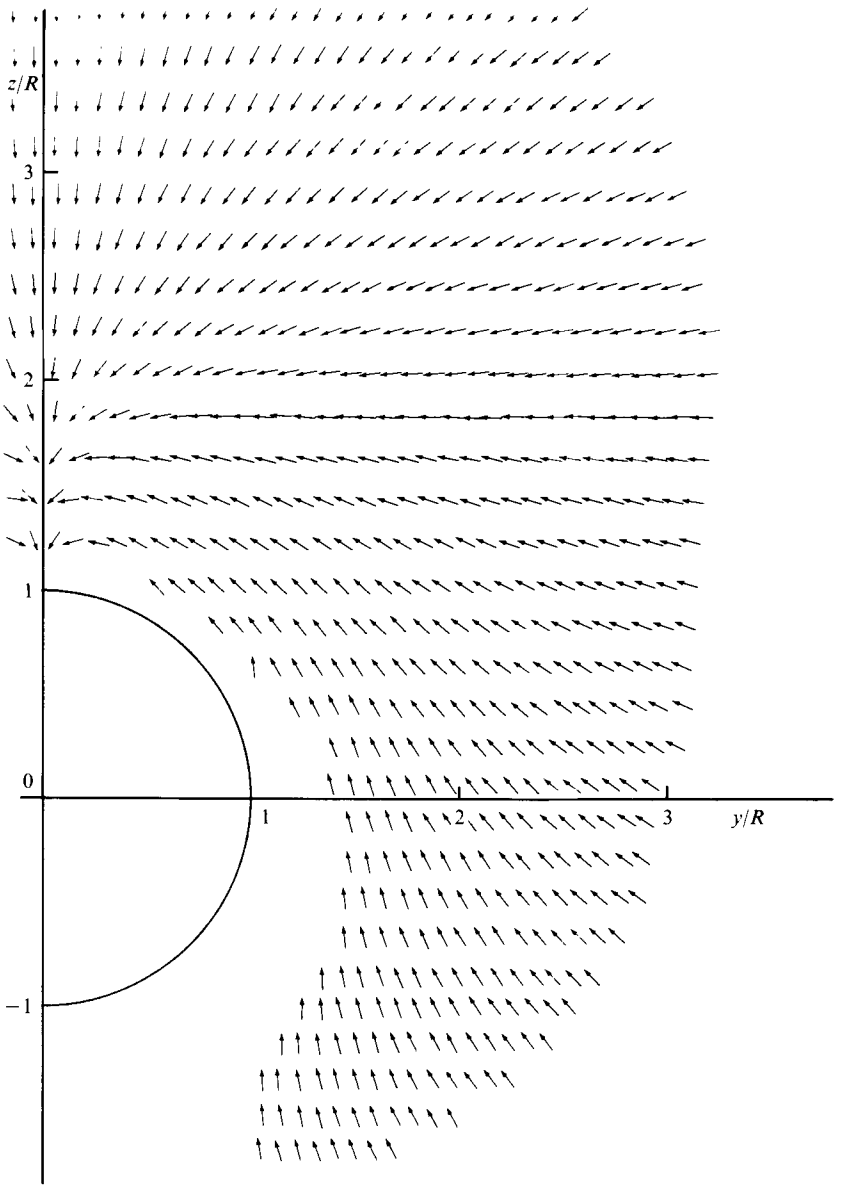

FIGURE 12. Direction of conical streamlines at $\alpha = 12{\cdot}4°$.

supersonic pocket terminated by the embedded shock wave seems to be comparable to the two-dimensional transonic flow problem in the case of an aerofoil, where no such an extended region is observed. The occurrence of anomalies in the measurements is rather unlikely, because at higher incidences this second supersonic region is much larger and seems to be a fundamental part of the flow field. The results of a numerical calculation of the flow field by a shock-capturing technique proposed by Kutler & Lomax (1971) are given in figure 11. The supersonic regime is more extended and the region of the shock wave is situated closer to the plane of symmetry than in the

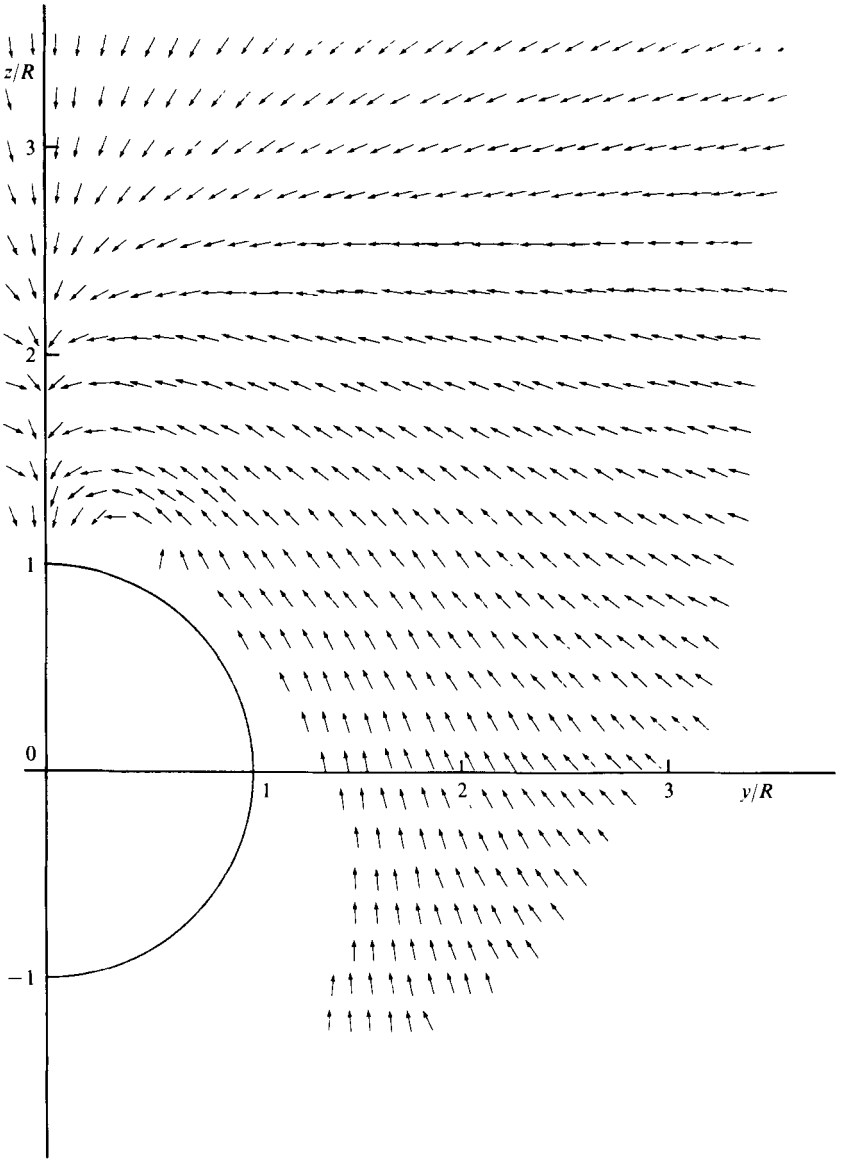

FIGURE 13. Direction of conical streamlines at $\alpha = 17{\cdot}3°$.

experiments. No second supersonic region downstream of the shock wave occurs in the calculated field. It is obvious that the development of a vortex near the plane of symmetry has a strong influence on the nature of the flow field and that in numerical calculations viscous effects should be taken into account.

Figure 8 shows the results of the measurements at $\alpha = 22{\cdot}4°$. This figure bears a strong qualitative resemblance to the results obtained at $\alpha = 17{\cdot}3°$, but the conical supersonic regime is much larger. Also, a third supersonic regime is measured, extending across the symmetry plane just above the cone. Proceeding towards the cone surface, the region begins with a conical sonic line and ends with a shock wave normal to the

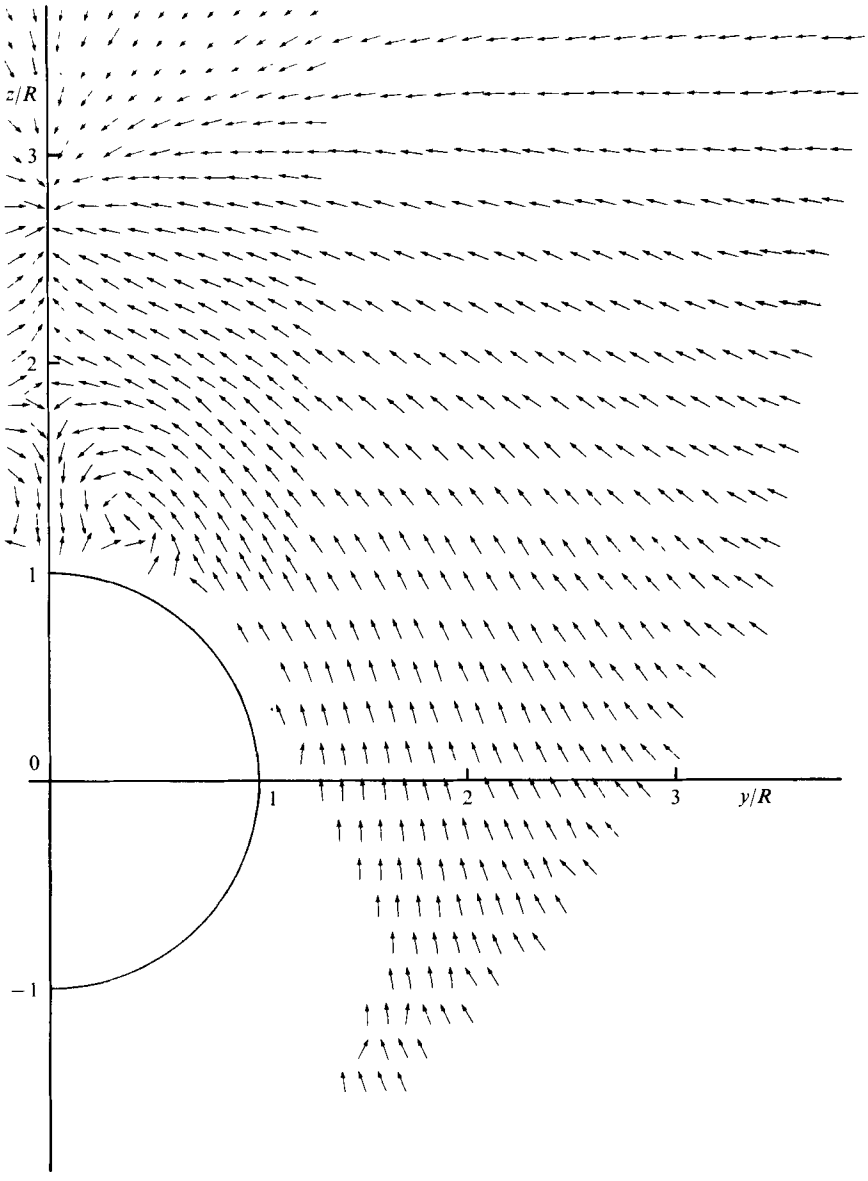

FIGURE 14. Direction of conical streamlines at $\alpha = 22{\cdot}4°$.

symmetry plane. In the schlieren picture in figure 10 the shock wave is shown as a very straight line emanating from the cone apex, suggesting that the vortices generating the shock wave are of a conical character.

Flow directions. The conical velocity distribution measured at an angle of incidence of 12·4° is given in figure 12. The length of the pointers is not related to the magnitude of the conical velocity. Linearized inviscid flow calculations by Bakker & Bannink (1974) show the existence of a conical stagnation point in the plane of symmetry, away from the cone surface; the measurements also show a stagnation point, although it is not lifted off the body. The measured conical velocity in the leeward symmetry

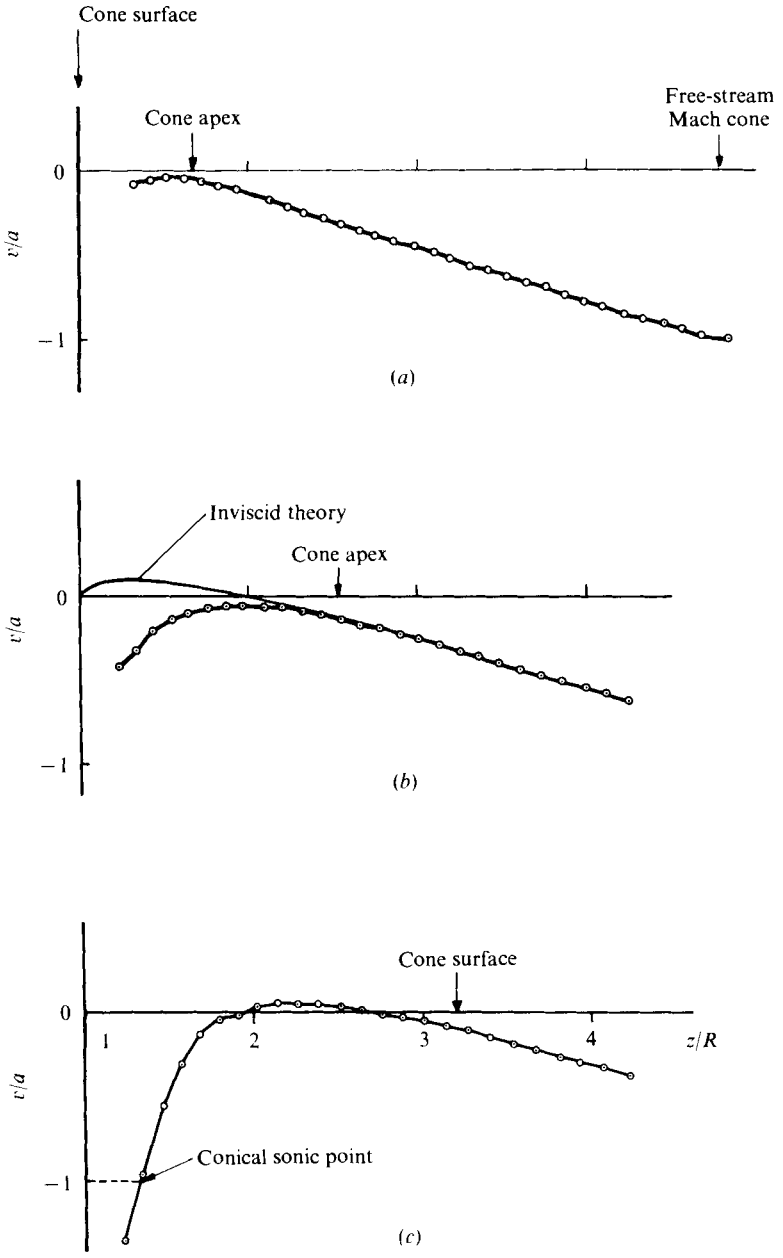

FIGURE 15. Conical velocity distribution in the leeward plane of symmetry. (*a*) $\alpha = 12{\cdot}4°$, (*b*) $\alpha = 17{\cdot}3°$, (*c*) $\alpha = 22{\cdot}4°$.

plane remains negative (see figures 12 and 15*a*); consequently no conical stagnation points are found away from the cone surface.

On comparing figures 12 and 13 it follows that at $\alpha = 17{\cdot}3°$ the flow structure has not changed essentially from that at $\alpha = 12{\cdot}4°$. The conical stagnation point is still located on the cone surface. As suggested by Houwink & Nebbeling (1975), the strength of the leeward vortices apparently has great influence on the appearance of conical stagnation

points in the flow field. For inviscid flow, numerical calculations predict a conical stagnation point well away from the body surface at $\alpha = 17{\cdot}3°$; see figure 15(*b*), where the measured data have also been presented. The calculated stagnation point is located well below the intersection of the free-stream velocity vector with the z/R axis (the 'cone apex' in figure 15*b*). However, the measured values of v/a in the plane of symmetry remain negative for all values of z.

At an incidence of 22·4° (figure 14), the flow field has changed into one with a stagnation point away from the cone surface at $z/R = 2{\cdot}7$ and with a fully developed vortex system near the plane of symmetry. In addition, a near-wake stagnation point is found at a value of z/R of about 1·9. At this point the dividing streamline ends. In the plane of symmetry the conical velocity v/a twice assumes the value $v/a = 0$ (figure 15*c*). Near the cone surface the velocity increases up to Mach numbers greater than one ($v/a < -1$). As has been seen already, the deceleration towards the cone surface occurs in part via a shock wave.

It should be mentioned that the flow-direction measurements close to the cone surface are not very accurate as a result of probe–surface interference.

6. Concluding remarks

The detailed flow-direction measurements described in the present article, which were obtained using a carefully calibrated probe, extend the information available so far on the viscous flow about circular cones. The existing knowledge on this complex subject relies mainly on experimental work. For moderate angles of incidence, the analyses by Lubard & Helliwell (1973) and Bontoux & Roux (1975) show that very adequate numerical methods have been developed to describe the flow field. For large angles of incidence ($\alpha > 2\theta_c$) no theoretical results are available for the viscous flow. In particular, the complex vortex system causes great difficulty. In general the results of the present measurements agree very well with those of Rainbird (1968), Feldhuhn & Winkelmann (1969), Feldhuhn *et al.* (1970) and Houwink (1974). The extension given here concerns the determination of conical supersonic regions, conical sonic lines and detailed flow directions.

A new feature revealed by the present investigation is the peculiar shape of the embedded shock wave due to interaction of the viscous, separated inner flow and the outer, essentially inviscid part of the flow field. In addition, the measurements leave no doubt about the existence of leeward vortices. Refined measurements are necessary to obtain better information on the precise structure of the vortex core and the existence of secondary vortices. The streamline pattern measured close to the vortex core should be regarded as only qualitative because of the size of the probe.

Although the main purpose of the measurements has been the investigation of the flow field away from the cone surface, a fine-interval determination of the surface pressure is considered necessary to obtain a complete picture of the flow past the cone. Precision surface pressure measurements, together with a refined investigation of the flow direction, will be the object of further research in the near future.

The authors are very grateful to Mr O. J. Anema for the efficient preparation of the computer program used for the reduction of the data and for his assistance in obtaining the final results. The assistance rendered by Mr J. Boeker in the preparation of the manuscript is greatly appreciated.

Appendix. Calibration of the probe

An extensive calibration of the conical-head probe provides the means of determining all local flow quantities if the total temperature of the flow is known. The flow angle with respect to the probe axis is related to the pressure differences across the two sets of opposite pressure orifices, non-dimensionalized by the local Pitot pressure. These pressure differences depend also on the local Mach number, which may vary from point to point in the flow field (Andrews & Sawyer 1963). The local Mach number is derived from the calibrated ratio of the central-hole pressure p_5 to the average of the four cone surface pressures $p_1, \ldots, p_4$. This ratio is a function of the Mach number and of the inclination of the velocity vector with respect to the probe axis. It is clear that an iterative process is required to obtain both the Mach number and the flow direction from the pressure measurements. A number of factors influencing the accuracy of the results should be taken into account:

(*a*) The pressure p_5 measured by the central hole may differ at large flow angles from the Pitot pressure. A correction may thus be required.

(*b*) Owing to the finite number of pressure orifices on the conical probe surface, the average of the measured pressures is not necessarily equal to the mean surface pressure. At a given Mach number, the mean surface pressure depends only on the flow angle with respect to the probe axis and not on the roll angle of the probe. The average of the four surface pressures depends also on the relative circumferential position of the pressure holes with respect to the velocity vector. Fortunately, it was found that this effect could be neglected if the total incidence of the probe did not exceed 20°.

(*c*) The ratio of the Pitot pressure to the surface pressure depends strongly on the semi-apex angle of the conical probe head. This means that a local convergence or divergence of the flow may lead to a misinterpretation of the Mach number. As the derivation of the flow direction is only weakly dependent on the local Mach number, the ensuing error in the flow direction is small. These errors are largely eliminated by the interpolation procedure described below.

(*d*) In the presence of transverse pressure gradients, errors in the measurement of the flow direction are introduced by the finite dimensions of the probe. To compensate for these errors, an interpolation scheme has been used in the data reduction. The measured surface pressures have been interpolated to the value that would have been obtained if the pressure hole had been located on the axis of the probe.

The calibration of the probe was carried out in the TST 27 wind tunnel at Mach numbers $M = 2{\cdot}2$, $M = 2{\cdot}97$ and $M = 3{\cdot}5$. The probe was mounted on a variable-pitch support. The calibration started with the two static pressure orifices 1 and 2 (see figure 1) in the vertical symmetry plane (the plane in which the angle of incidence is varied). During a run at constant stagnation pressure, the incidence of the probe was varied in steps of 1° from $-2°$ to 16°. After each step the five probe pressures and the angle of incidence were read. The whole run was computer controlled. A 'time-lag decision procedure' was built into the computer program: each transducer was repeatedly read out and the output accepted and recorded as soon as it had reached a stable value, indicating that pressure equalization had been obtained in the transducer. Subsequent runs were made with the probe rolled along its axis by multiples of 45° up to 315°. The entire procedure was repeated for the other Mach numbers.

The measured data are expressed as pressure functions, i.e. functions relating the

pressure differences across opposite orifices to the true angle of pitch θ of the probe relative to the flow direction:

$$(p_2-p_1)/p_5 = f_1(\theta), \quad (p_4-p_3)/p_5 = f_2(\theta),$$

at constant values of the Mach number M and of the roll angle ϕ of the probe; p_1, p_2, p_3 and p_4 are the surface pressures on the conical part of the probe and p_5 is the pressure measured by the axial orifice. Owing to imperfections of the probe, $f_1(\theta)$ and $f_2(\theta)$ differ from zero for $\theta = 0$. The functions $f_1(\theta)$ and $f_2(\theta)$ are approximated by a general form in terms of θ as

$$F_1(\theta) = A_0 + A_1\theta + A_2\theta^2, \tag{A 1}$$

$$F_2(\theta) = B_0 + B_1\theta + B_2\theta^2. \tag{A 2}$$

The coefficients A_0, A_1, A_2, B_0, B_1 and B_2 are functions of ϕ and M; A_0 and B_0 are attributed to probe imperfections.

At any particular value of θ, the relation between $(p_2-p_1)/p_5$ and $(p_4-p_3)/p_5$ may be expressed by the relation of a so-called super-ellipse:

$$\left[\frac{(p_2-p_1)/p_5 - [A_0]_{\phi=0}}{[F_1(\theta)-A_0]_{\phi=0}}\right]^{n(\theta)} + \left[\frac{(p_4-p_3)/p_5 - [B_0]_{\phi=90°}}{[F_2(\theta)-B_0]_{\phi=90°}}\right]^{n(\theta)} = 1, \tag{A 3}$$

where the exponent n is a calibrated function of θ and is close to the value 2. It should be pointed out that, owing to probe imperfections, different values of $n(\theta)$ are obtained for the four quadrants of the super-ellipse. The calibration results of the probe are not exactly equal to the results (provided with a minus sign) of the upside-down calibration. As a result, the calibration curve obtained consists of four super-ellipse segments that are not exactly symmetrical with respect to the horizontal and vertical axes.

The calibration curves were obtained at the three Mach numbers mentioned above for θ increments of 1°, so that for the expected range of Mach numbers in the cone flow field a fair set of curves was available.

The Mach number may be obtained from the ratio of the mean value of the four surface pressures to the pressure p_5 measured by the axial orifice. At zero incidence of the probe the Mach number may be found from the ratio

$$(p_1+p_2+p_3+p_4)/4p_5 = F_3(M). \tag{A 4}$$

As the pressure ratio $(p_1+p_2+p_3+p_4)/4p_5$ is a function of not only the Mach number but also the angle of incidence θ, the next function to be determined from the calibrations is

$$(p_1+p_2+p_3+p_4)/4p_5 = F_4(\theta) \text{ at } M = \text{constant}. \tag{A 5}$$

The function $F_4(\theta)$ is used as a correction to $F_3(M)$. In principle, $F_4(\theta)$ depends also on the roll angle ϕ, however it was found that for angles θ less than 20° the influence of ϕ on F_4 may be neglected. During the actual measurements in the flow field of the cone, the probe was mounted such that the maximum flow inclination with respect to the probe was less than 20° at any place in the flow field. The local static pressure in the flow field will be determined from the Mach number and the local Pitot pressure. In general the flow will be inclined to the probe, therefore the measured pressure p_5 has to be corrected in order to obtain the Pitot pressure. So a function

$$p_p/p_5 = F_5(\theta) \tag{A 6}$$

has to be determined from the calibrations at each of the three Mach numbers. From the known functions $F_1, \ldots, F_5$ and the measured total temperature, all flow quantities may be determined from flow-field measurements to a high degree of accuracy.

REFERENCES

ANDREWS, D. R. & SAWYER, W. G. 1963 *Aero. Res. Counc. Current Paper* no. 628.

BAKKER, P. G. & BANNINK, W. J. 1974 *Dept. Aerospace Engng, Delft Univ. Tech., Rep.* VTH-184.

BONTOUX, P. & ROUX, B. 1975 *A.I.A.A. Paper* no. 75–858.

FELDHUHN, R. H. & WINKELMANN, A. E. 1969 *Naval Ordnance Lab., White Oak, Md, Rep.* NOL-TR-69-36.

FELDHUHN, R. H., WINKELMANN, A. E. & PASIUK, L. 1970 *A.I.A.A. Paper* no. 70–766.

FLETCHER, C. A. J. 1975 *Proc. 4th Int. Conf. Num. Meth. Fluid Dyn. Lecture Notes in Physics*, vol. 35, pp. 161–166. Springer.

GUFFROY, D., ROUX, B., MARCILLAT, J., BRUN, R. & VALENSI, J. 1968 *Agard Conf. Proc.* no. 30, paper 20.

HOLT, M. & NDEFO, D. E. 1970 *J. Comp. Phys.* **5**, 463–486.

HOUWINK, R. 1974 *Dept. Aerospace Engng., Delft Univ. Tech., Rep.* VTH-168.

HOUWINK, R. & NEBBELING, C. 1975 *Delft Prog. Rep.* C **1**, 69–76.

JONES, D. J. 1969 *AGARDograph* no. 137.

KUTLER, P. & LOMAX, H. 1971 *A.I.A.A. Paper* no. 71–99.

LUBARD, S. C. & HELLIWELL, W. S. 1973 *A.I.A.A. Paper* no. 73–636.

MASSOT, P. 1976 Thèse de doctorat, Université d'Aix-Marseille.

NAKAO, S. I. 1975 *Inst. Space Aero. Sci., Univ. Tokyo, Rep.* no. 534.

RAINBIRD, W. J. 1968 *AGARD Conf. Proc.* no. 30, paper 19.

STETSON, K. F. 1972 *A.I.A.A. J.* **10**, 642–648.

TRACY, R. R. 1963 *Aero. Lab., Cal. Inst. Tech., Memo.* no. 69.

YAHALOM, R. 1971 *Aero. Sci. Div., Univ. California, Berkeley, Rep.* AFOSR-TR-71-2183.

ZAKKAY, V. & ALZNER, E. 1974 *Air Force Flight Dyn. Lab., Wright-Patterson AFB, Ohio, Rep.* AFFDL-TR-74-19.

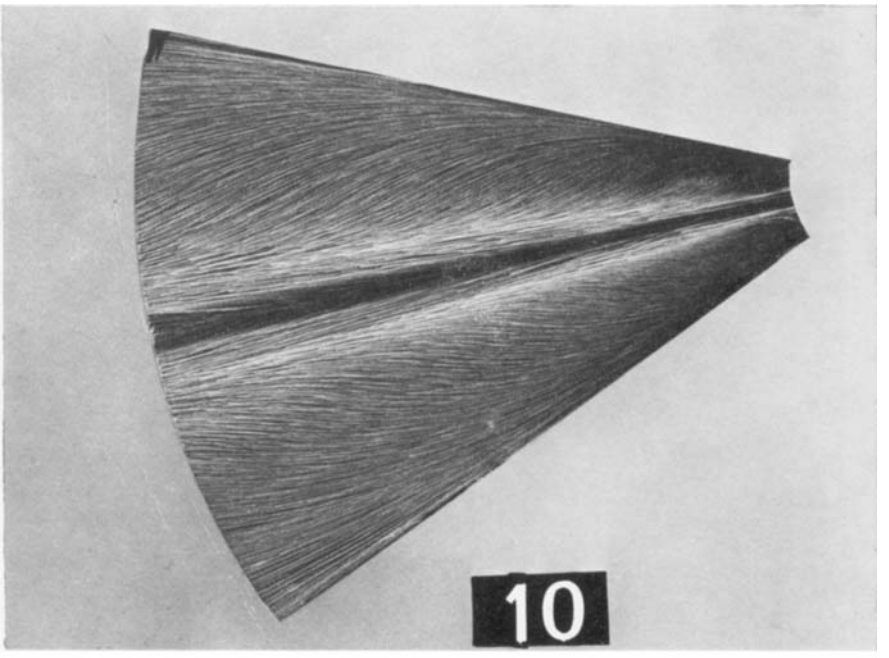

(*a*)

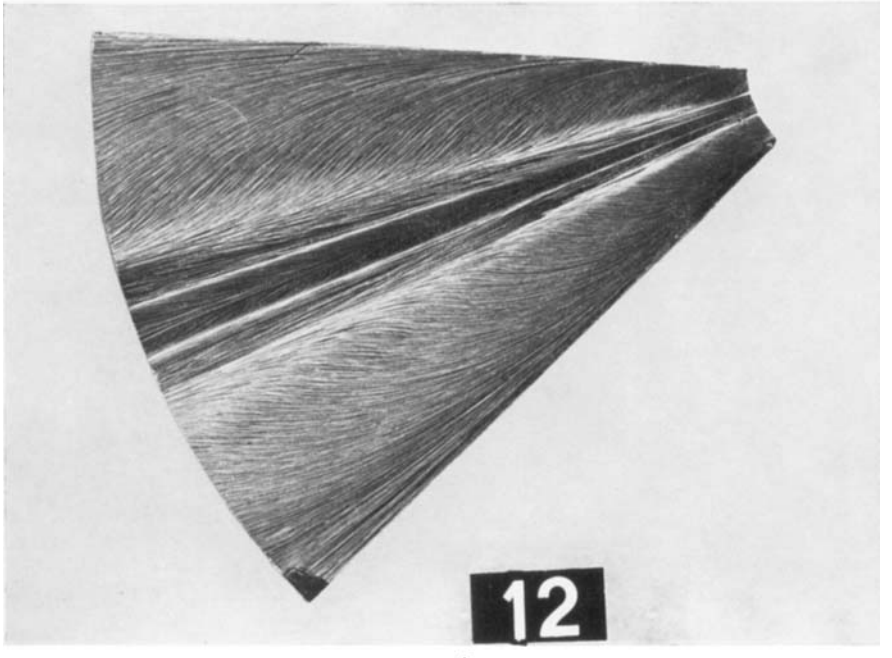

(*b*)

FIGURES 3(*a*, *b*). For legend see plate 2.

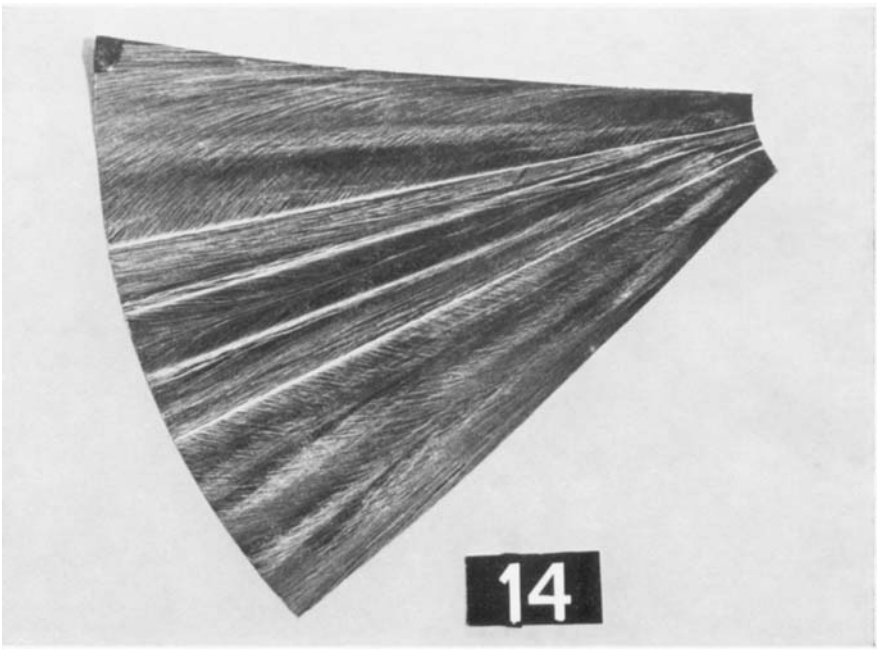

(*c*)

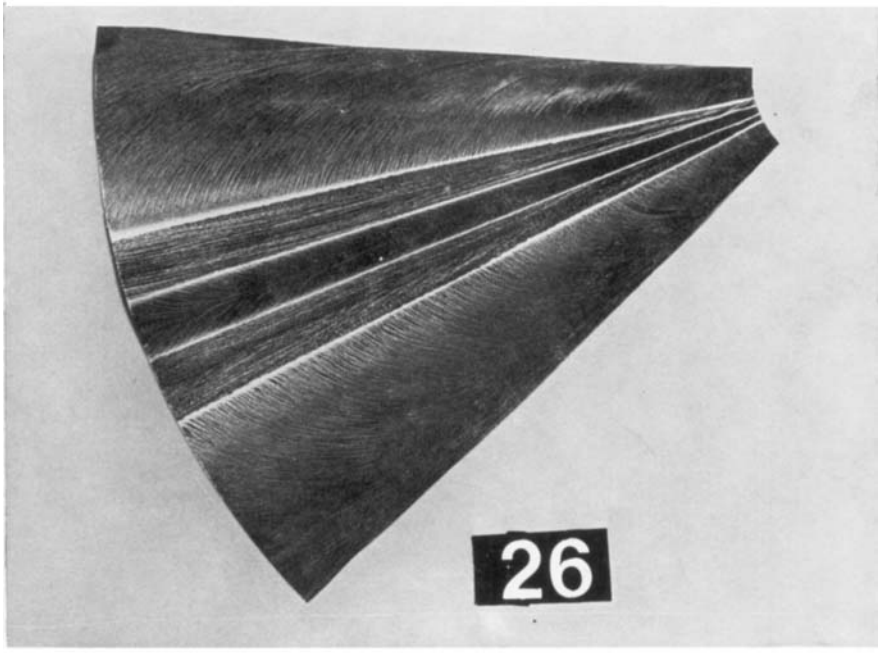

(*d*)

FIGURE 3. Oil-flow patterns at cone surface. (*a*) $\alpha = 10°$, (*b*) $\alpha = 12°$, (*c*) $\alpha = 14°$, (*d*) $\alpha = 26°$.

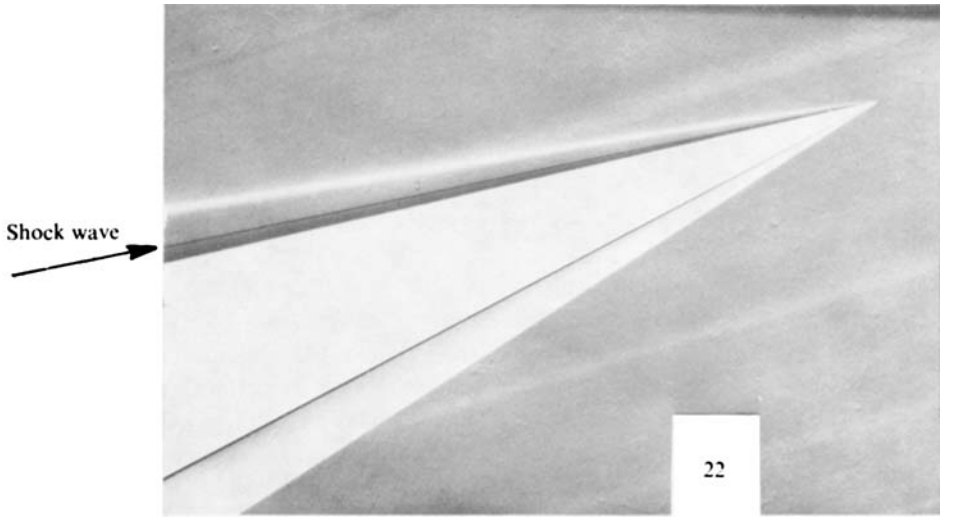

FIGURE 10. Schlieren picture of the cone at $\alpha = 22{\cdot}4°$.